Geophys. J. Int. (2002) **149,** 508–523

The edge dislocation problem in a layered elastic medium

Eleonora Rivalta, Walter Mangiavillano and Maurizio Bonafede

Department of Physics, University of Bologna, viale Berti-Pichat 8-40127 *Bologna, Italy. E-mail: bonafede@ibogfs.df.unibo.it*

Accepted 2001 November 13. Received 2001 November 13; in original form 2001 February 7

SUMMARY

Analytic solutions are provided for the displacement and stress fields induced by an edge dislocation in a layered medium composed of two welded half-spaces endowed with different elastic parameters. A plane strain configuration is considered, with the dislocation surface perpendicular to the interface between the two half-spaces. Two cases are considered: in case I the dislocation surface is entirely embedded in one half-space, in case II the dislocation surface cuts across the interface. From these elementary solutions, a closed Volterra dislocation (with constant slip) can be easily obtained: in model A the dislocation opens and closes within the same medium, in model B it opens in one half-space and closes in the other. These elementary solutions also provide the singular kernel of the integral equation governing the equilibrium configuration of a mode-II crack (in which the stress drop is assigned). The stress field induced by closed Volterra dislocations (models A and B) or by a crack with constant stress drop (model C) is computed and compared with the solutions in a homogeneous medium. Important differences appear in the overall pattern of the stress maps. Lower values are generally found for the vertical normal component and for the shear component near and within the softer half-space, which might be anticipated on intuitive grounds as due to the different rigidity of the two media in welded contact. However, unexpected differences are found in the normal stress component parallel to the interface (which needs not be continuous at the interface): this component shows wide regions of high stress on the hard side of the interface which, in models B and C, give rise to clear maxima and minima within two narrow lobes elongated along the interface. These interface stress concentrations extend up to distances comparable to the vertical extension of the dislocation surface and their amplitude is comparable to the stress change induced over the dislocation surface. The physical motivation for the presence of these maxima are discussed and their dependence is studied from the rigidity contrast between the two media and from the position of the dislocation surface relative to the interface.

Key words: dip-slip fault, dislocations, heterogeneous media.

INTRODUCTION

In recent years, fault interaction has been widely recognized as being responsible for important contributions to the stress field. These interactions may alter significantly the undisturbed seismic cycle, by anticipating, delaying or even triggering earthquakes on nearby faults (e.g. Stein *et al.* 1992; King *et al.* 1994; Harris 1998).

The displacement and the stress fields generated by the slip of transform, thrust or normal faults are usually estimated through the solutions of the elastostatic equation for screw or edge dislocations. These studies have been performed mostly employing homogeneous half-space models, for which a complete set of analytical solutions is available (Okada 1992), in spite of the presence of considerable heterogeneities within the Earth's crust (e.g. the sedimentary-basement transition or the upper-lower crust transition). Heterogeneous (layered models) have been mostly developed for point sources, (e.g. Singh 1970; Rundle 1980; Roth 1990) owing to the mathematical difficulties arising when tackling with extended sources. An extended source is often modelled through a discrete distribution of point sources but, due to the strong singularities present in the stress field of a point source, this procedure is non-convergent near the source and is thus unsuitable for near-field studies (e.g. Bonafede & Rivalta 1999b).

In order to overcome these problems, numerical methods have become more popular than the analytic ones. Finite element or boundary element methods are more versatile and allow us to take into account different aspects, such as structural heterogeneities (e.g. Crouch & Starfield 1990; Dahm 1996) or surface topography (e.g. Savage & Swalfs 1986; McTigue & Segall 1988), in order to obtain models closer to reality.

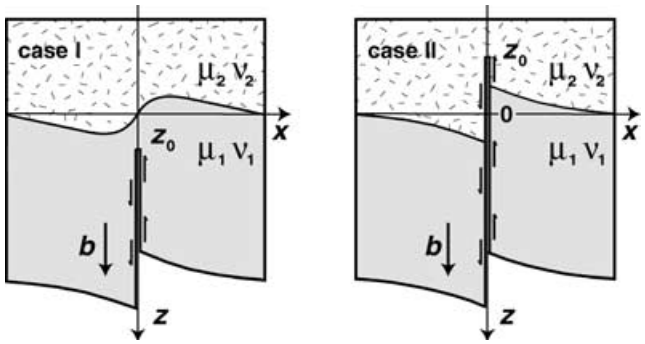

Figure 1. Sketch of the elementary dislocation problem in a layered medium. The lower half-space, in $z > 0$, is endowed with Poisson ratio ν_1 and rigidity μ_1; it is welded to the 'upper' half-space in $z < 0$ (Poisson ratio ν_2 and rigidity μ_2) along the plane $z = 0$. A dip-slip dislocation line is present in $x = 0, z = z_0$ with Burgers vector $\mathbf{b} = b\mathbf{k}$. The dislocation surface goes from $z = z_0$ to $z = +\infty$: the face $x = 0^+$ of the dislocation surface is displaced in the z-direction by $-b/2$, the face $x = 0^-$ is displaced by the same amount in the opposite direction. Case I: the dislocation line is in the half-space 1 ($z_0 > 0$). Case II: the dislocation line is in the half-space 2 ($z_0 < 0$).

Nevertheless, numerical methods face some problems, such as difficulties in handling singularities (and dislocation problems are intrinsically singular) or in choosing the most appropriate boundary conditions: this problem is particularly relevant in heterogeneous media where boundary conditions must be assigned even at interfaces within the computational domain. The validation of numerical models is thus strictly connected with their capability of reproducing the analytical solutions available for the problem closest to that of interest.

Analytical solutions of dislocation problems in layered media are also important for more general reasons: exact solutions of simplified models provide a basic understanding of the physical problem under study, even if they may be unsuitable for application to specific real cases. Moreover, solving the dislocation equations analytically, permits us to extract the singular kernel appearing in the integral equation which govern crack equilibrium.

In this paper we complete the analysis of the dislocation problems in layered media, begun with the study of tensile dislocations and cracks (Bonafede & Rivalta 1999a,b) and of screw dislocations and cracks (Rybicki 1971; Bonafede *et al.* 2002). We proceed now with the application of the previous investigation techniques to the remaining case of the edge dislocation, in which the Burger's vector is parallel to the dislocation surface and perpendicular to the dislocation line (Fig. 1). We shall restrict to considering the case of a dislocation surface perpendicular to the interface between the two media, since solutions for oblique surfaces can be obtained as linear combinations of tensile dislocations and edge dislocations over vertical surfaces.

Analytic solutions in closed form will be obtained for the displacement and stress fields generated by a vertical edge dislocation with constant slip (Burgers vector), in the proximity of (case I) or across (case II) the interface between two different elastic media. Over the interface $z = 0$, displacement and traction components are imposed to be continuous (welded boundary conditions). Edge dislocations present several mathematical analogies with the previously analysed case of tensile dislocations (Bonafede & Rivalta 1999a, hereafter termed as Paper I), so that the solutions will be expressed in terms of the previously defined constants and functions retaining the same symbol convention, whenever possible.

THE ELEMENTARY EDGE DISLOCATION

Let us consider an elementary edge dislocation, embedded in a medium, made up of two half-spaces, characterized by different elastic parameters and welded along the plane interface $z = 0$ (Fig. 1). We assume a plane strain configuration in which no dependence from the coordinate y is allowed and the displacement vanishes in the y-direction. The elementary dislocation surface is defined as the half-plane $x = 0, z > z_0$, bounded by the dislocation line $x = 0, z = z_0$. Over the dislocation surface, a jump discontinuity of the displacement $\mathbf{u}$ is assigned, which is described by a constant Burger's vector $\mathbf{b} = b\mathbf{k}$

$$-b_i = u_i(x = 0^+, z) - u_i(x = 0^-, z), \qquad z > z_0$$

(the minus sign being due to convention). If the solutions pertinent to an unbounded homogeneous medium are used separately in each half-space, employing the elastic parameters pertinent to each half-space, the interface $z = 0$ is the site of discontinuities for the displacement and the stress fields; some of these discontinuities must be removed to comply with the welded boundary conditions. The aim of the following paragraph is to compute the stress and displacement fields generated in the half-space $z > 0$ and in the half-space $z < 0$ by assigned surface tractions presenting the same discontinuities; subtracting these expressions (termed Galerkin contributions) from the homogeneous dislocation solutions will provide the final solutions in which displacements and tractions are continuous across the interface.

To this end the Galerkin method will be employed (e.g. Fung 1965), which permits us to deduce the stress and displacement fields produced in a half-space $z > 0$ (or $z < 0$) by the imposition of assigned loads on the surface $z = 0$.

The dislocation line is $x = 0, z = z_0$, which is parallel to the y-axis and the Burgers vector $\mathbf{b} = b\hat{\mathbf{k}}$ is constant. Apart from an arbitrary rigid body translation, the edge-dislocation solution in an unbounded medium can be written as (e.g. Landau & Lifschitz 1967)

$$\begin{cases} u_x^{(\infty)}(x,z,z_0) = -\dfrac{b}{4\pi(1-\nu)}\left[(1-2\nu)\ln\sqrt{\dfrac{x^2+(z-z_0)^2}{z_0^2}} + \dfrac{(z-z_0)^2}{x^2+(z-z_0)^2}\right] \\ u_z^{(\infty)}(x,z,z_0) = -\dfrac{b}{2\pi}\left[\phi(x,z;z_0) - \dfrac{1}{2(1-\nu)}\dfrac{x(z-z_0)}{x^2+(z-z_0)^2}\right] \end{cases} \tag{1}$$

where the superscript (∞) indicates that this is the solution for a homogeneous unbounded medium and

$$\phi(x,z;z_0) = \begin{cases} \dfrac{\pi}{2} + \arctan\dfrac{z-z_0}{x} & \text{if} \quad x > 0 \\ -\dfrac{\pi}{2} + \arctan\dfrac{z-z_0}{x} & \text{if} \quad x < 0. \end{cases} \tag{2}$$

The stress field induced by this displacement is given by the following expressions:

$$\begin{cases} \sigma_{xx}^{(\infty)}(x,z,z_0) = \dfrac{b\mu}{2\pi(1-\nu)}\dfrac{x\left[(z-z_0)^2-x^2\right]}{\left[x^2+(z-z_0)^2\right]^2} \\ \sigma_{xz}^{(\infty)}(x,z,z_0) = \dfrac{b\mu}{2\pi(1-\nu)}\dfrac{(z-z_0)\left[(z-z_0)^2-x^2\right]}{\left[x^2+(z-z_0)^2\right]^2} \\ \sigma_{zz}^{(\infty)}(x,z,z_0) = -\dfrac{b\mu}{2\pi(1-\nu)}\dfrac{x\left[x^2+3(z-z_0)^2\right]}{\left[x^2+(z-z_0)^2\right]^2} \\ \sigma_{yy}^{(\infty)}(x,z,z_0) = -\dfrac{b\mu\nu}{\pi(1-\nu)}\dfrac{x}{x^2+(z-z_0)^2}. \end{cases} \tag{3}$$

Substituting μ_1, ν_1 for μ, ν in the half-space $z > 0$ and μ_2, ν_2 in the half-space $z < 0$, the following discontinuities of the displacement and traction components would appear in $z = 0$:

$$\begin{cases} \Delta u_x(x,z_0) = u_{x2}^{(\infty)}(x,z_0) - u_{x1}^{(\infty)}(x,z_0) = b\gamma\left[\ln\sqrt{\dfrac{x^2+z_0^2}{z_0^2}} - \dfrac{z_0^2}{x^2+z_0^2}\right] \\ \Delta u_z(x,z_0) = u_{z2}^{(\infty)}(x,z_0) - u_{z1}^{(\infty)}(x,z_0) = b\gamma\dfrac{xz_0}{x^2+z_0^2} \end{cases} \tag{4}$$

$$\begin{cases} \Delta\sigma_{xz}(x,z_0) = \sigma_{xz2}^{(\infty)}(x,z_0) - \sigma_{xz1}^{(\infty)}(x,z_0) = b\delta\dfrac{z_0\left[x^2-z_0^2\right]}{\left[x^2+z_0^2\right]^2} \\ \Delta\sigma_{zz}(x,z_0) = \sigma_{zz2}^{(\infty)}(x,z_0) - \sigma_{zz1}^{(\infty)}(x,z_0) = -b\delta\dfrac{x\left[x^2+3z_0^2\right]}{\left[x^2+z_0^2\right]^2} \end{cases} \tag{5}$$

where subscripts 1 and 2 refer to the half-spaces $z > 0$ and $z < 0$, respectively, and

$$\begin{aligned} \gamma_1 &= \frac{1}{4\pi}\frac{1}{(1-\nu_1)}, & \delta_1 &= \frac{1}{2\pi}\frac{\mu_1}{(1-\nu_1)} \\ \gamma_2 &= \frac{1}{4\pi}\frac{1}{(1-\nu_2)}, & \delta_2 &= \frac{1}{2\pi}\frac{\mu_2}{(1-\nu_2)} \\ \gamma &= \gamma_2 - \gamma_1, & \delta &= \delta_2 - \delta_1. \end{aligned} \tag{6}$$

Since the welded interface is normal to the z-axis, the continuity of tractions implies the continuity of σ_{zx} and σ_{zz} (σ_{zy} vanishes identically in plane strain). Discontinuities of σ_{xx} and σ_{yy} must not be removed.

The process involved in the computation of the Galerkin components has already been detailed in Bonafede & Rivalta (1999a) for the tensile dislocation problem; accordingly, intermediate results, necessary to obtain the final expressions, are reported here only in the case of differences. The first step is computing the Fourier transforms of the discontinuities to be removed.

Fourier components of discontinuities (case I)

In the case $z_0 > 0$, we may write the discontinuities (4) and (5) in terms of their Fourier transforms:

$$\begin{cases} \Delta\sigma_{zz}(x,z_0) = -b\delta\dfrac{x\left[x^2+3z_0^2\right]}{\left[z_0^2+x^2\right]^2} = b\delta\displaystyle\int_0^{+\infty}\eta(k)\sin kx\,dk \\ \Delta\sigma_{xz}(x,z_0) = -b\delta\dfrac{z_0\left[z_0^2-x^2\right]}{\left[z_0^2+x^2\right]^2} = b\delta\displaystyle\int_0^{+\infty}\xi(k)\cos kx\,dk \\ \Delta\dfrac{\partial u_x}{\partial x}(x,z_0) = b\gamma\dfrac{x\left[x^2+3z_0^2\right]}{\left[z_0^2+x^2\right]^2} = -b\gamma\displaystyle\int_0^{+\infty}\eta(k)\sin kx\,dk \\ \Delta\dfrac{\partial u_z}{\partial x}(x,z_0) = -b\gamma\dfrac{z_0\left[z_0^2-x^2\right]}{\left[z_0^2+x^2\right]^2} = b\gamma\displaystyle\int_0^{+\infty}\xi(k)\cos kx\,dk \end{cases} \tag{7}$$

where the Fourier transforms $\eta(k)$ and $\xi(k)$ are easily computed employing the theorem of residues:

$$\begin{cases} \xi(k) = kz_0e^{-kz_0} \\ \eta(k) = (1+kz_0)e^{-kz_0} \qquad z_0>0. \end{cases} \tag{8}$$

The derivatives of the displacement are employed above, instead of the displacement itself, since the latter is non-integrable over $0<x<\infty$ (so that its F-transform does not exist).

The Galerkin components (case I)

The dislocation line is $x=0, z=z_0>0$. Let us compute the displacement and stress fields generated in the half-spaces $z>0$ and $z<0$ by assigned harmonically modulated tractions $\tilde\sigma_{ij}^G$ over the plane $z=0$. A superposed tilde designates a single harmonic component and the superscript G reminds us that this is the Galerkin contribution. For a detailed description of the Galerkin method, employed here for removing the discontinuities on the interface, we refer to Bonafede & Rivalta (1999a). The present problems require the following boundary conditions (the first set is for the Galerkin problem in half-space 1, the second for half-space 2):

$$\begin{cases} \tilde\sigma_{zz1}^G(x,z=0) = A_1(k)\sin kx \\ \tilde\sigma_{xz1}^G(x,z=0) = B_1(k)\cos kx \\ \tilde\sigma_{yz1}^G(x,z=0) = 0 \\ \tilde\sigma_{ij1}^G(z\to+\infty) = 0 \quad \forall i,j. \end{cases} \qquad \begin{cases} \tilde\sigma_{zz2}^G(x,z=0) = A_2(k)\sin kx \\ \tilde\sigma_{xz2}^G(x,z=0) = B_2(k)\cos kx \\ \tilde\sigma_{yz2}^G(x,z=0) = 0 \\ \tilde\sigma_{ij2}^G(z\to-\infty) = 0 \quad \forall i,j. \end{cases} \tag{9}$$

where $A_1(k),\ldots,B_2(k)$ are functions of the wavenumber k to be determined.

The displacement components arising from the boundary conditions above are obtained after integrating the following expressions with respect to x:

$$\begin{cases} \dfrac{\partial\tilde u_{x1}^G}{\partial x} = \dfrac{e^{-kz}\sin kx}{2\mu_1}[(1-2\nu_1)A_1(k)+2(1-\nu_1)B_1(k)-[A_1(k)+B_1(k)]kz] \\ \dfrac{\partial\tilde u_{x2}^G}{\partial x} = \dfrac{e^{kz}\sin kx}{2\mu_2}[(1-2\nu_2)A_2(k)-2(1-\nu_2)B_2(k)+[A_2(k)-B_2(k)]kz] \\ \dfrac{\partial\tilde u_{z1}^G}{\partial x} = \dfrac{e^{-kz}\cos kx}{2\mu_1}[2(1-\nu_1)A_1(k)+(1-2\nu_1)B_1(k)+[A_1(k)+B_1(k)]kz] \\ \dfrac{\partial\tilde u_{z2}^G}{\partial x} = \dfrac{e^{kz}\cos kx}{2\mu_2}[-2(1-\nu_2)A_2(k)+(1-2\nu_2)B_2(k)+[A_2(k)-B_2(k)]kz]. \end{cases} \tag{10}$$

The stress components generated by the same loads are:

$$\begin{cases} \tilde\sigma_{zz1}^G(x,z;k) = [A_1(k)+(A_1(k)+B_1(k))kz]e^{-kz}\sin kx \\ \tilde\sigma_{zz2}^G(x,z;k) = [A_2(k)-(A_2(k)-B_2(k))kz]e^{kz}\sin kx \\ \tilde\sigma_{xz1}^G(x,z;k) = [B_1(k)-(A_1(k)+B_1(k))kz]e^{-kz}\cos kx \\ \tilde\sigma_{xz2}^G(x,z;k) = [B_2(k)-(A_2(k)-B_2(k))kz]e^{kz}\cos kx \\ \tilde\sigma_{xx1}^G(x,z;k) = [A_1(k)+2B_1(k)-(A_1(k)+B_1(k))kz]e^{-kz}\sin kx \\ \tilde\sigma_{xx2}^G(x,z;k) = [A_2(k)-2B_2(k)+(A_2(k)-B_2(k))kz]e^{kz}\sin kx \\ \tilde\sigma_{yy1}^G(x,z;k) = 2\nu_1(A_1(k)+B_1(k))e^{-kz}\sin kx \\ \tilde\sigma_{yy2}^G(x,z;k) = 2\nu_2(A_2(k)-B_2(k))e^{kz}\sin kx. \end{cases} \tag{11}$$

We can now arrange a linear system to determine the coefficients A_1, A_2, B_1, B_2, which are required to remove the harmonic components of the discontinuities in (7):

$$\mathbf{M}\begin{pmatrix} A_2 \\ A_1 \\ B_2 \\ B_1 \end{pmatrix} = b\begin{pmatrix} \delta\eta(k) \\ \delta\xi(k) \\ -\gamma\eta(k) \\ \gamma\xi(k) \end{pmatrix} \tag{12}$$

where $\xi(k)$ and $\eta(k)$ are given by (8) and the matrix $\mathbf{M}$ in the present case becomes:

$$\mathbf{M} = \begin{pmatrix} 1 & -1 & 0 & 0 \\ 0 & 0 & 1 & -1 \\ \dfrac{1-2\nu_2}{2\mu_2} & -\dfrac{1-2\nu_1}{2\mu_1} & -\dfrac{1-\nu_2}{\mu_2} & -\dfrac{1-\nu_1}{\mu_1} \\ \dfrac{1-\nu_2}{\mu_2} & \dfrac{1-\nu_1}{\mu_1} & -\dfrac{1-2\nu_2}{2\mu_2} & \dfrac{1-2\nu_1}{2\mu_1} \end{pmatrix}. \tag{13}$$

Hence

$$(A_2, A_1, B_2, B_1)^T = b\mathbf{M}^{-1}(\delta\eta(k), \delta\xi(k), -\gamma\eta(k), \gamma\xi(k))^T \tag{14}$$

The inverse matrix $\mathbf{M}^{-1}$ can be written as

$$\mathbf{M}^{-1} = \frac{1}{(e-d)(e+d)}\begin{pmatrix} -(a_1+c^+) & c^- & d & -e \\ (a_2+c^+) & c^- & d & -e \\ c^- & -(a_1+c^+) & e & -d \\ c^- & (a_2+c^+) & e & -d \end{pmatrix} \tag{15}$$

where

$$\begin{cases} a_1 = \dfrac{3-4\nu_1}{4\mu_1^2} & a_2 = \dfrac{3-4\nu_2}{4\mu_2^2} \\ c^- = \dfrac{1-(3-4\nu_1)(3-4\nu_2)}{8\mu_1\mu_2} & c^+ = \dfrac{1+(3-4\nu_1)(3-4\nu_2)}{8\mu_1\mu_2} \\ d = \dfrac{1-2\nu_2}{2\mu_2} - \dfrac{1-2\nu_1}{2\mu_1} & e = \dfrac{1-\nu_2}{\mu_2} + \dfrac{1-\nu_1}{\mu_1} \end{cases}. \tag{16}$$

From (15) we can compute analytically the coefficients $A_1(k)$, $A_2(k)$, $B_1(k)$, $B_2(k)$ as functions of the wavenumber k. These will be inserted into (11) and, after integrating in dk, we obtain the stress fields σ_{ij}^G generated by the discontinuities (7). The integrals $I_{ij}(x, z; z_0)$ involved in synthesizing the response of the two half-spaces to the discontinuities (7) are the same as those defined in Bonafede & Rivalta (1999a) for the tensile dislocation problem and are reproduced here in Appendix A.

Employing these definitions of I_{ij} the solution can be written most simply by defining a row matrix $\vec{\sigma}^G$

$$\vec{\sigma}^G = \begin{pmatrix} \sigma_{xz1}^G & \sigma_{xz2}^G & \sigma_{zz1}^G & \sigma_{zz2}^G \end{pmatrix} \tag{17}$$

Obtaining the following expressions:

$$\sigma_i^G = b\sum_{j=1}^{4} F_{ij}^I I_{ij}, \quad \text{(no sum over } i\text{)}. \tag{18}$$

where superscript 'I' denotes case I and

$$\mathbf{F^I} = \begin{pmatrix} D & C_2 - D & -(C_2 - D) & 2(C_2 - D) \\ D & C_1 + D & -(C_1 - D) & 0 \\ -C_2 & -(C_2 - D) & -(C_2 - D) & -2(C_2 - D) \\ -C_1 & C_1 + D & -(C_1 - D) & 0 \end{pmatrix}. \tag{19}$$

with

$$\begin{cases} C_1 = \dfrac{1}{(e^2-d^2)}[\delta(a_1+c^+)+\gamma d] \\ C_2 = \dfrac{1}{(e^2-d^2)}[-\delta(a_2+c^+)+\gamma d]\ . \\ D\ = \dfrac{1}{(e^2-d^2)}[\delta c^- - \gamma e] \end{cases} \tag{20}$$

a_1, a_2, c^-, c^+, d, e being defined in (16) and δ, γ in (6).

A simpler expression for C_1, C_2 and D directly in terms of the elastic parameters $\nu_1, \nu_2, \mu_1, \mu_2$ can be obtained after some algebraic manipulation:

$$\begin{cases} C_1 = \delta_2 - 2\mu_1\mu_2(\kappa_1+\kappa_2) \\ C_2 = \delta_1 - 2\mu_1\mu_2(\kappa_1+\kappa_2)\ . \\ D\ = 2\mu_1\mu_2(\kappa_1-\kappa_2) \end{cases} \tag{21}$$

where δ_1 and δ_2 are given in (6) and

$$\begin{cases} \kappa_1 = \dfrac{1}{2\pi}\dfrac{1}{\mu_1+(3-4\nu_1)\mu_2} \\ \kappa_2 = \dfrac{1}{2\pi}\dfrac{1}{\mu_2+(3-4\nu_2)\mu_1} \end{cases}\ . \tag{22}$$

Other stress components (which need not be continuous on $z=0$) complete the specification of the stress tensor:

$$\begin{cases} \dfrac{1}{b}\sigma^G_{xx1} = -(C_2-2D)I_{31} + (C_2-D)I_{32} - 3(C_2-D)I_{33} + 2(C_2-D)I_{34} \\ \dfrac{1}{b}\sigma^G_{xx2} = -(C_1+2D)I_{41} - (C_1+D)I_{42} + (C_1-D)I_{43} \\ \dfrac{1}{b}\sigma^G_{yy1} = -2\nu_1(C_2-D)(I_{31}+2I_{33}) \\ \dfrac{1}{b}\sigma^G_{yy2} = -2\nu_2(C_1+D)I_{41} \end{cases} \tag{23}$$

Analytic expressions for the displacement components are finally obtained by integrating (10) in dk and then in dx; the following primitives are needed:

$$Y_{ij}(x,z;z_0) = \int I_{ij}(x,z;z_0)\,dx$$

and the integration constant is chosen in such a way as to make the displacement continuous across the interface. These primitives have been computed in Bonafede & Rivalta (1999a) and are reproduced here in Appendix A.

Galerkin contributions to the displacement components for case I, due to the strain function, accordingly are:

$$\begin{cases} u^G_{x1}(x,z;z_0) = b\displaystyle\sum_{j=1}^{4} T^I_{3j}Y_{3j}(x,z;z_0) \\ u^G_{x2}(x,z;z_0) = b\displaystyle\sum_{j=1}^{4} T^I_{4j}Y_{4j}(x,z;z_0) \\ u^G_{z1}(x,z;z_0) = b\displaystyle\sum_{j=1}^{4} T^I_{1j}Y_{1j}(x,z;z_0) \\ u^G_{z2}(x,z;z_0) = b\displaystyle\sum_{j=1}^{4} T^I_{2j}Y_{2j}(x,z;z_0) \end{cases} \tag{24}$$

where $\mathbf{T^I}$ is the following matrix:

$$\mathbf{T^I} = \begin{pmatrix} \mu_1\kappa_1-\mu_2\kappa_2 & \gamma_1-2\mu_2\kappa_1 & -\gamma_1+2\mu_1\kappa_1 & 2(\gamma_1-2\mu_2\kappa_1) \\ \mu_1\kappa_1-\mu_2\kappa_2 & \gamma_2-2\mu_1\kappa_2 & -\gamma_2+2\mu_1\kappa_1 & 0 \\ \gamma_1-\mu_1\kappa_1-\mu_2\kappa_2 & \gamma_1-2\mu_2\kappa_1 & \gamma_1-2\mu_1\kappa_1 & 2(\gamma_1-2\mu_2\kappa_1) \\ \gamma_2-\mu_1\kappa_1-\mu_2\kappa_2 & -(\gamma_2-2\mu_1\kappa_2) & \gamma_2-2\mu_1\kappa_1 & 0 \end{pmatrix} \tag{25}$$

and $\gamma_1, \gamma_2, \kappa_1, \kappa_2$ are given in (6) and (22).

Thus we have obtained the complete set of solutions for the Galerkin problems in half-space $z > 0$ and $z < 0$ when $z_0 > 0$ (case I). The elementary dislocation solutions $u_{i1}^{(el)}$, $u_{i2}^{(el)}$, and $\sigma_{ij1}^{(el)}$, $\sigma_{ij2}^{(el)}$ in a medium formed by two welded half-spaces is obtained after subtracting the Galerkin displacement u_i^G and stress σ_{ij}^G, from the dislocation solutions in a homogeneous unbounded medium $u_i^{(\infty)}$ and $\sigma_{ij}^{(\infty)}$ (eqs 1–2):

$$u_{i1}^{(el)} = u_{i1}^{(\infty)} - u_{i1}^G, \quad \sigma_{ij1}^{(el)} = \sigma_{ij1}^{(\infty)} - \sigma_{ij1}^G, \quad \text{in} \quad z > 0$$
$$u_{i2}^{(el)} = u_{i2}^{(\infty)} - u_{i2}^G, \quad \sigma_{ij2}^{(el)} = \sigma_{ij2}^{(\infty)} - \sigma_{ij2}^G, \quad \text{in} \quad z < 0.$$

The problem of case II, in which $z_0 < 0$, can be solved employing the same procedure sketched above. We skip the details and write down the complete elementary solutions in the next paragraph, superfix (*el*) will be omitted henceforth.

ELEMENTARY SOLUTIONS

Case I

According to what has been exposed in the previous paragraph, the displacement field generated by an elementary dip-slip dislocation in a layered medium, when $z_0 > 0$, is:

$$\begin{cases} \dfrac{1}{b}u_{x1}(x,z,z_0) = -\dfrac{1}{4\pi(1-\nu_1)}\left[(1-2\nu_1)\ln\sqrt{\dfrac{x^2+(z-z_0)^2}{z_0^2}} + \dfrac{(z-z_0)^2}{x^2+(z-z_0)^2}\right] - \sum_{j=1}^{4} T_{3j}^I Y_{3j} \\ \dfrac{1}{b}u_{x2}(x,z,z_0) = -\dfrac{1}{4\pi(1-\nu_2)}\left[(1-2\nu_2)\ln\sqrt{\dfrac{x^2+(z-z_0)^2}{z_0^2}} + \dfrac{(z-z_0)^2}{x^2+(z-z_0)^2}\right] - \sum_{j=1}^{4} T_{4j}^I Y_{4j} \\ \dfrac{1}{b}u_{z1}(x,z,z_0) = -\dfrac{1}{2\pi}\left[\Phi(x,z;z_0) - \dfrac{1}{2(1-\nu_1)}\dfrac{x(z-z_0)}{x^2+(z-z_0)^2}\right] - \sum_{j=1}^{4} T_{1j}^I Y_{1j} \\ \dfrac{1}{b}u_{z2}(x,z,z_0) = -\dfrac{1}{2\pi}\left[\Phi(x,z;z_0) - \dfrac{1}{2(1-\nu_2)}\dfrac{x(z-z_0)}{x^2+(z-z_0)^2}\right] - \sum_{j=1}^{4} T_{2j}^I Y_{2j} \end{cases} \tag{26}$$

where $\Phi(x,z;z_0)$ is given by (2), $Y_{ij}(x,z;z_0)$ are given in Appendix A and the matrix $\mathbf{T^I}$ is given by (25). Stress components for which the continuity conditions were imposed are given by

$$\begin{cases} \dfrac{1}{b}\sigma_{zz1}(x,z,z_0) = -\dfrac{\mu_1}{2\pi(1-\nu_1)}\dfrac{x\left[x^2+3(z-z_0)^2\right]}{\left[x^2+(z-z_0)^2\right]^2} - \sum_{j=1}^{4} F_{3j}^I I_{3j} \\ \dfrac{1}{b}\sigma_{zz2}(x,z,z_0) = -\dfrac{\mu_2}{2\pi(1-\nu_2)}\dfrac{x\left[x^2+3(z-z_0)^2\right]}{\left[x^2+(z-z_0)^2\right]^2} - \sum_{j=1}^{4} F_{4j}^I I_{4j} \\ \dfrac{1}{b}\sigma_{xz1}(x,z,z_0) = \dfrac{\mu_1}{2\pi(1-\nu_1)}\dfrac{(z-z_0)\left[(z-z_0)^2-x^2\right]}{\left[x^2+(z-z_0)^2\right]^2} - \sum_{j=1}^{4} F_{1j}^I I_{1j} \\ \dfrac{1}{b}\sigma_{xz2}(x,z,z_0) = \dfrac{\mu_2}{2\pi(1-\nu_2)}\dfrac{(z-z_0)\left[(z-z_0)^2-x^2\right]}{\left[x^2+(z-z_0)^2\right]^2} - \sum_{j=1}^{4} F_{2j}^I I_{2j} \end{cases} \tag{27}$$

where $I_{ij}(x,z;z_0)$ are given in Appendix A and $\mathbf{F^I}$ is given by (19). Other non-vanishing stress components are

$$\begin{cases} \dfrac{1}{b}\sigma_{xx1}(x,z,z_0) = \dfrac{\mu_1}{2\pi(1-\nu_1)}\dfrac{x\left[(z-z_0)^2-x^2\right]}{\left[x^2+(z-z_0)^2\right]^2} + (C_2-2D)I_{31} - (C_2-D)I_{32} + 3(C_2-D)I_{33} - 2(C_2-D)I_{34} \\ \dfrac{1}{b}\sigma_{xx2}(x,z,z_0) = \dfrac{\mu_2}{2\pi(1-\nu_2)}\dfrac{x\left[(z-z_0)^2-x^2\right]}{\left[x^2+(z-z_0)^2\right]^2} + (C_1+2D)I_{41} + (C_1+D)I_{42} - (C_1-D)I_{43} \\ \dfrac{1}{b}\sigma_{yy1}(x,z,z_0) = -\dfrac{\mu_1\nu_1}{\pi(1-\nu_1)}\dfrac{x}{x^2+(z-z_0)^2} + 2\nu_1(C_2-D)(I_{31}+2I_{33}) \\ \dfrac{1}{b}\sigma_{yy2}(x,z,z_0) = -\dfrac{\mu_2\nu_2}{\pi(1-\nu_2)}\dfrac{x}{x^2+(z-z_0)^2} + 2\nu_2(C_1+D)I_{41} \end{cases} . \tag{28}$$

where C_1, C_2, D are given by (20) or (21).

Case II

If the dislocation surface extends from $z = z_0 < 0$ to $z = +\infty$ (i.e. if it cuts the interface $z = 0$), the displacement field is given by:

$$\begin{cases} \dfrac{1}{b}u_{x1}(x,z,z_0) = -\dfrac{1}{4\pi(1-\nu_1)}\left[(1-2\nu_1)\ln\sqrt{\dfrac{x^2+(z-z_0)^2}{z_0^2}} + \dfrac{(z-z_0)^2}{x^2+(z-z_0)^2}\right] - \sum_{j=1}^{4} T_{4j}^{II} Y_{4j} \\ \dfrac{1}{b}u_{x2}(x,z,z_0) = -\dfrac{1}{4\pi(1-\nu_2)}\left[(1-2\nu_2)\ln\sqrt{\dfrac{x^2+(z-z_0)^2}{z_0^2}} + \dfrac{(z-z_0)^2}{x^2+(z-z_0)^2}\right] - \sum_{j=1}^{4} T_{3j}^{II} Y_{3j} \\ \dfrac{1}{b}u_{z1}(x,z,z_0) = -\dfrac{1}{2\pi}\left[\Phi(x,z;z_0) - \dfrac{1}{2(1-\nu_1)}\dfrac{x(z-z_0)}{x^2+(z-z_0)^2}\right] - \sum_{j=1}^{4} T_{2j}^{II} Y_{2j} \\ \dfrac{1}{b}u_{z2}(x,z,z_0) = -\dfrac{1}{2\pi}\left[\Phi(x,z;z_0) - \dfrac{1}{2(1-\nu_2)}\dfrac{x(z-z_0)}{x^2+(z-z_0)^2}\right] - \sum_{j=1}^{4} T_{1j}^{II} Y_{1j} \end{cases} . \tag{29}$$

where

$$\mathbf{T^{II}} = \begin{pmatrix} -(\mu_1\kappa_1 - \mu_2\kappa_2) & \gamma_2 - 2\mu_1\kappa_2 & -(\gamma_2 - 2\mu_2\kappa_2) & 2(\gamma_2 - 2\mu_1\kappa_2) \\ -(\mu_1\kappa_1 - \mu_2\kappa_2) & \gamma_1 - 2\mu_2\kappa_1 & -(\gamma_1 - 2\mu_2\kappa_2) & 0 \\ \gamma_2 - \mu_1\kappa_1 - \mu_2\kappa_2 & \gamma_2 - 2\mu_1\kappa_2 & \gamma_2 - 2\mu_2\kappa_2 & 2(\gamma_2 - 2\mu_1\kappa_2) \\ \gamma_1 - \mu_1\kappa_1 - \mu_2\kappa_2 & -(\gamma_1 - 2\mu_2\kappa_1) & \gamma_1 - 2\mu_2\kappa_2 & 0 \end{pmatrix} . \tag{30}$$

We may note that (29) and (30) can be obtained respectively from (24) and (25) by keeping the same expressions for the unbounded medium solution and exchanging the roles of half-spaces 1 and 2 (i.e. $x \to -x, z \to -z, \mu_1 \to \mu_2$ and $\nu_1 \to \nu_2$) in the second part of the solution. Indeed if such an exchange is performed, we must also change, from (21), $C_1 \to C_2$, $C_2 \to C_1$, $D \to -D$. It might be proved that these selection rules must hold, employing invariance arguments and the superposition principle.

Stress components on which the continuity conditions are imposed are given by

$$\begin{cases} \dfrac{1}{b}\sigma_{zz1}(x,z,z_0) = -\dfrac{\mu_1}{2\pi(1-\nu_1)}\dfrac{x\left[x^2+3(z-z_0)^2\right]}{\left[x^2+(z-z_0)^2\right]^2} - \sum_{j=1}^{4} F_{4j}^{II} I_{4j} \\ \dfrac{1}{b}\sigma_{zz2}(x,z,z_0) = -\dfrac{\mu_2}{2\pi(1-\nu_2)}\dfrac{x\left[x^2+3(z-z_0)^2\right]}{\left[x^2+(z-z_0)^2\right]^2} - \sum_{j=1}^{4} F_{3j}^{II} I_{3j} \\ \dfrac{1}{b}\sigma_{xz1}(x,z,z_0) = \dfrac{\mu_1}{2\pi(1-\nu_1)}\dfrac{(z-z_0)\left[(z-z_0)^2-x^2\right]}{\left[x^2+(z-z_0)^2\right]^2} - \sum_{j=1}^{4} F_{2j}^{II} I_{2j} \\ \dfrac{1}{b}\sigma_{xz2}(x,z,z_0) = \dfrac{\mu_2}{2\pi(1-\nu_2)}\dfrac{(z-z_0)\left[(z-z_0)^2-x^2\right]}{\left[x^2+(z-z_0)^2\right]^2} - \sum_{j=1}^{4} F_{1j}^{II} I_{1j} \end{cases} . \tag{31}$$

where

$$\mathbf{F^{II}} = \begin{pmatrix} -D & C_1 + D & -(C_1 + D) & 2(C_1 + D) \\ -D & C_2 - D & -(C_2 + D) & 0 \\ -C_1 & -(C_1 + D) & -(C_1 + D) & -2(C_1 + D) \\ -C_2 & C_2 - D & -(C_2 + D) & 0 \end{pmatrix} . \tag{32}$$

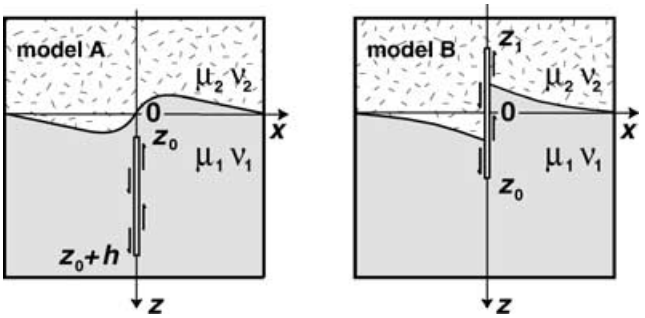

Figure 2. A closed Volterra dislocation is obtained by superposing the elementary solution for a dislocation line in $z = z_0$ and Burgers vector b with the solution for a dislocation line in $z = z_0 + h$ and Burgers vector $-b$. In model A the dislocation surface is entirely embedded in half-space 1. In model B the dislocation surface cuts across the interface from $z_1 < 0$ to $z_0 > 0$ ($z_0 - z_1 = h = 10$ km).

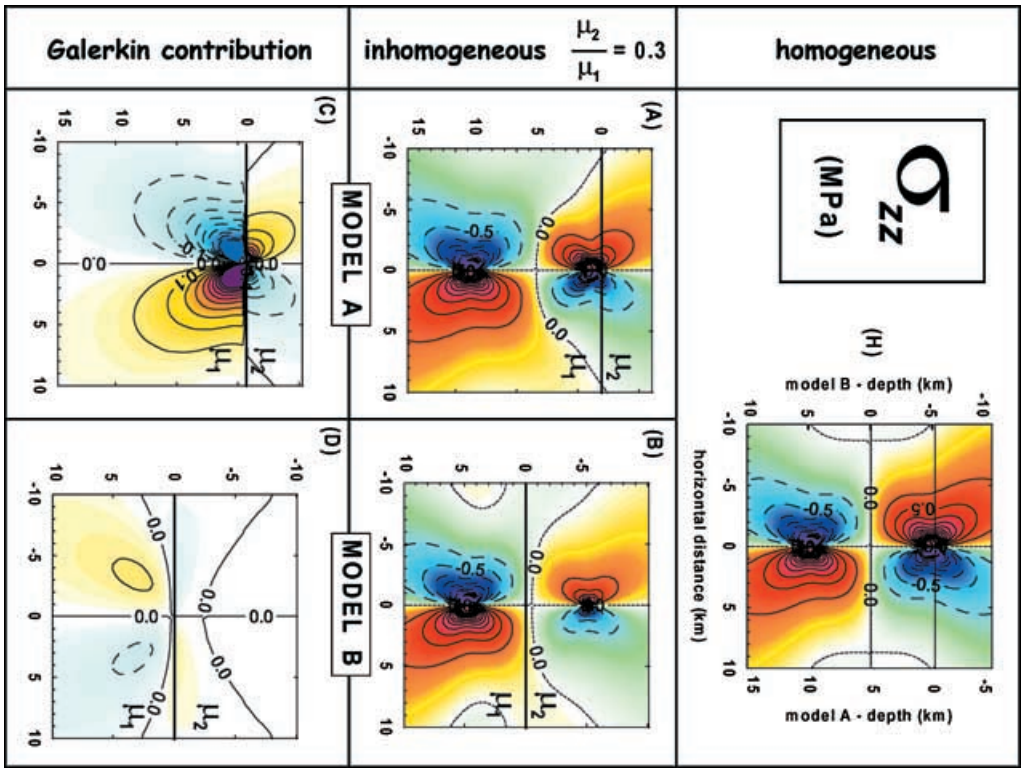

Figure 3. Map of the stress component σ_{zz} (normal to the interface) for a bounded dislocation surface with vertical extension $h = 10$ km and Burgers vector $b = 30$ cm. Coordinates x and z are in km. Stress contours are plotted at 0.25 MPa intervals by solid lines if positive (tensile, yellow-to-red), by dashed lines if negative (compressive, green-to violet). (h) homogeneous medium with $\mu_2 = \mu_1 = 30$ GPa; the ordinate on the left refers to model B, the ordinate on the right to model A. (a) model A: $z_0 = 0.2$ km, $h = 10$ km, $\mu_1 = 30$ GPa and $\mu_2 = 0.3\mu_1$ ($\nu_1 = \nu_2 = 0.25$); the interface between half-spaces 1 and 2 is the plane $z = 0$, shown as a solid line. (b) model B: the interface is still in $z = 0$, elastic constants as in (a), dislocation surface $-h/2 < z < +h/2$ with $h = 10$ km. (c) Opposite of the Galerkin contribution $-\sigma_{zz}^G$ for model A, contour lines plotted at 0.05 MPa interval; (d) same as (c), for model B.

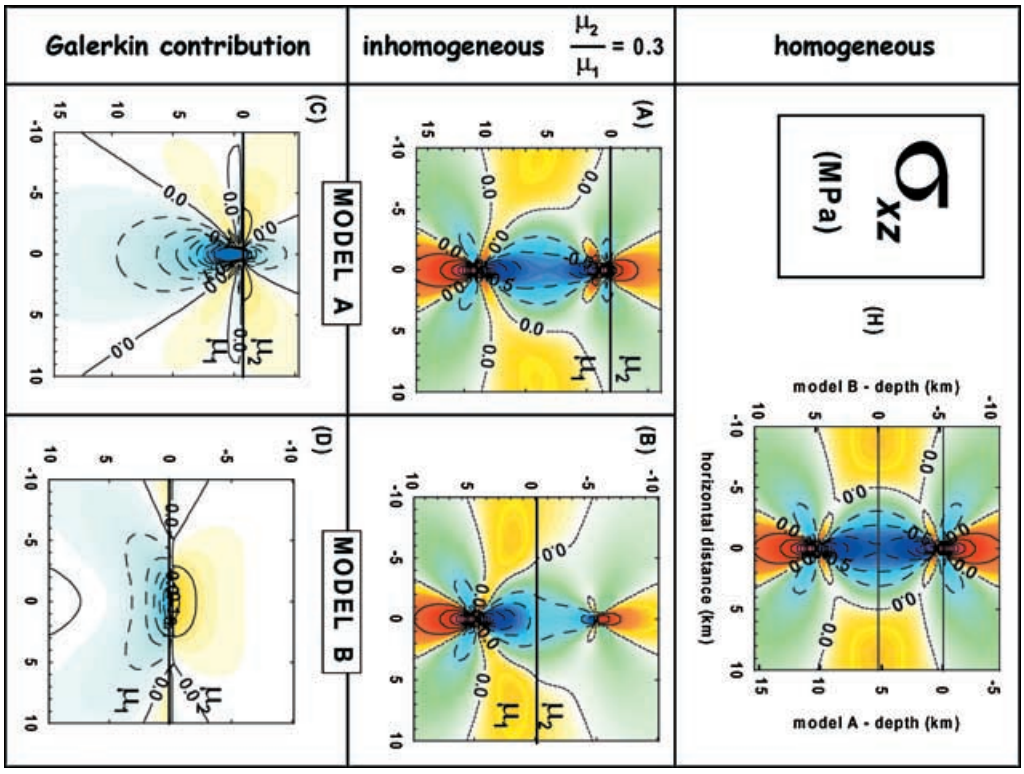

Figure 4. Same as Fig. 3 for the shear component σ_{xz}.

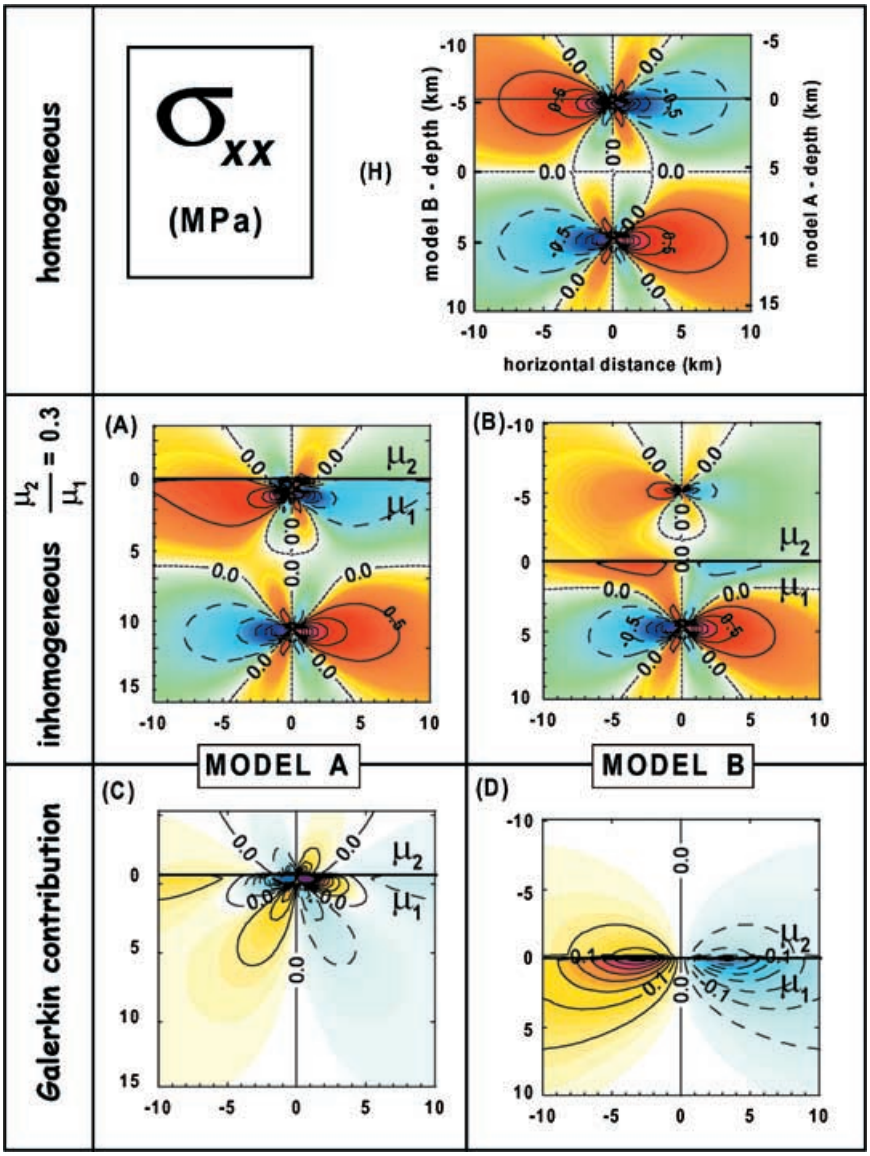

Figure 5. Same as Fig. 3 for the stress component σ_{xx}. Note the wide stress concentration near the interface in panels (a) and (b) and the sign reversal (with respect to the homogeneous medium) in panel (b) below the interface.

Other non-vanishing stress components are

$$\begin{cases} \dfrac{1}{b}\sigma_{xx1}(x,z,z_0) = \dfrac{\mu_1}{2\pi(1-\nu_1)}\dfrac{x\left[(z-z_0)^2-x^2\right]}{\left[x^2+(z-z_0)^2\right]^2} + (C_2-2D)I_{41} + (C_2-D)I_{42} - (C_2+D)I_{43} \\ \dfrac{1}{b}\sigma_{xx2}(x,z,z_0) = \dfrac{\mu_2}{2\pi(1-\nu_2)}\dfrac{x\left[(z-z_0)^2-x^2\right]}{\left[x^2+(z-z_0)^2\right]^2} + (C_1+2D)I_{31} - (C_1+D)I_{32} + 3(C_1+D)I_{33} - 2(C_1+D)I_{34} \\ \dfrac{1}{b}\sigma_{yy1}(x,z,z_0) = -\dfrac{\mu_1\nu_1}{\pi(1-\nu_1)}\dfrac{x}{x^2+(z-z_0)^2} + 2\nu_1(C_2-D)I_{41} \\ \dfrac{1}{b}\sigma_{yy2}(x,z,z_0) = -\dfrac{\mu_2\nu_2}{\pi(1-\nu_2)}\dfrac{x}{x^2+(z-z_0)^2} + 2\nu_2(C_1+D)\left(I_{31}+2I_{33}\right) \end{cases} . \quad (33)$$

RESULTS AND DISCUSSION

The elastostatic equation has been solved for the case of an edge dislocation embedded in an inhomogeneous medium composed of two welded elastic half-spaces. Edge dislocations are typically employed in geophysics to model dip-slip faults, but clearly can also be employed

to model the stress induced by a strike-slip fault impinging on a lateral inhomogeneity. However, for clarity of exposition, we shall refer in the following to the coordinate z as the 'depth' below the interface. The present solutions complete the set of tensile dislocations (modelling dikes or crevasses) and screw dislocations (modelling strike-slip faults) in layered media (see Bonafede & Rivalta 1999a; Rybicki 1971; Bonafede *et al.* 2002).

Once the stress field generated by elementary dislocations has been obtained, it is easy to compute the effects of a closed dislocation. In fact, employing the solution of Case I we can build a rectangular dislocation embedded in half-space 1, below the interface, by writing the solution for a dislocation line in $z_0 > 0$ and subtracting from it the solution for a dislocation line in $z_0 + h$ (model A, Fig. 2). If on the contrary we subtract the solution for Case I with dislocation line in $z_0 > 0$ from the solution of Case II with dislocation line in $z_1 < 0$, we obtain a rectangular dislocation closed symmetrically across the interface (model B, Fig. 2).

Moreover, by integrating the elementary solutions, multiplied by a suitable dislocation density distribution, we can obtain a crack model (model C) in which the stress-drop $\Delta\tau_{xz}$ is assigned over the crack plane $x = 0$ and the slip is variable over the dislocation surface. This procedure differs only in minor details from that described in Bonafede & Rivalta (1999b) for a tensile crack, and will be omitted here for conciseness.

The stress maps resulting from these three models will now be examined and compared with the stress maps in a homogeneous medium. In Figs 3, 4 and 5 the stress components σ_{zz}, σ_{xz} and σ_{xx} are plotted for a closed dislocation in a homogeneous medium with $\mu_2 = \mu_1$ (in panel H), and compared with solutions in an inhomogeneous medium, plotted in panels (A) and (B) respectively for model A and B. In both models A and B we assume $\mu_1 = 30$ GPa, $\mu_2 = 9$ GPa, $(\mu_2/\mu_1 = 0.3)$, $b = 30$ cm, $h = 10$ km. In model A $z_0 = 200$ m, in model B $z_1 = -h/2$ and $z_0 = h/2$.

The stress components σ_{zz} and σ_{xz} are continuous across the interface $z = 0$, as imposed by the welded boundary condition, while the horizontal stress component σ_{xx} in models A and B is clearly discontinuous in $z = 0$. In Fig. 3, the main effects induced by the heterogeneity is the stress decrease close to and within the softer medium in $z < 0$. Such a decrease can be qualitatively interpreted as due to the smaller rigidity of half-space 1 and to the continuity of σ_{zz} across the interface, which lowers the stress even in the stiffer half-space 1. In other terms,

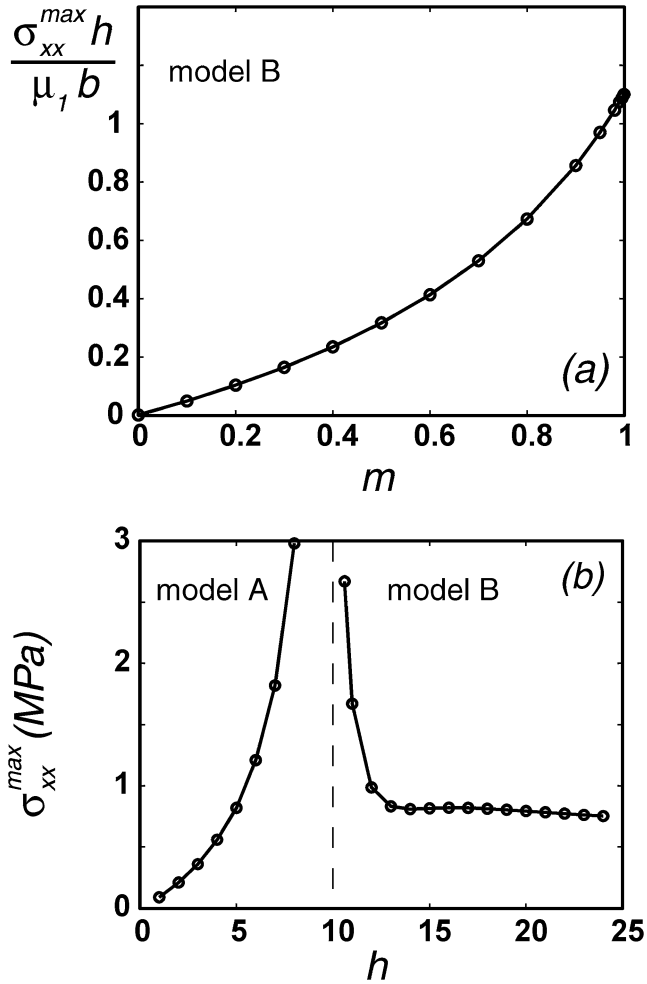

Figure 6. Maximum value of the Galerkin component $|\sigma_{xx}^{G}|$ over the interface $z = 0^{+}$. In (a) μ_2 is variable, while $z_1 = -5$ km, $z_0 = 5$ km, $\mu_1 = 30$ GPa, and $b = 30$ cm as in Fig. 3(b); stress values are normalized to $\frac{\mu_1 b}{h}$, (a representative stress drop value over the dislocation surface). In (b) h varies from 1 to 24 km, the dislocation surface is $z_0 - h < z < z_0$, with $z_0 = -10$ km, $\mu_1 = 30$ GPa, $\mu_2 = 0.3\mu_1$, $b = 30$ cm.

one might think that the strain field is practically unaffected by the presence of the heterogeneity so that the change in rigidity is the main cause of the stress changes with respect to the homogeneous case. But this is an oversimplification of the actual results, particularly close to the interface. In order to appreciate better the effects induced by the heterogeneity on the σ_{zz} component, $-\sigma_{zz}^{G}$ (the opposite of the Galerkin contribution) is plotted in panels (c) and (d) of Fig. 3 for model A and B respectively. This is the contribution to be added to the homogeneous solution $\sigma_{zz1}^{(\infty)}$ (in $z > 0$) and $\sigma_{zz2}^{(\infty)}$ (in $z < 0$) to obtain the complete solution. Fig. 3(c) shows that the introduction of the heterogeneity induces significant additional stress contributions close to the interface: these have the same sign as in the homogeneous model in the softer half-space 2 but the opposite sign in the harder half-space 1. Thus, in model A, the introduction of the heterogeneity enhances σ_{zz} in the softer medium and lowers it in the harder medium. This strong stress concentration is related to some terms of the Galerkin contribution becoming singular when both z and z_0 approach zero. Far away from the interface, the Galerkin contribution vanishes and the solution becomes more and more similar to the homogeneous solution.

In model B however, the Galerkin component is small, even close to the interface, so that the solution is indeed similar to $\sigma_{zz1}^{(\infty)}$ and $\sigma_{zz2}^{(\infty)}$ (Fig. 3d). This is clearly due to the larger distance of the dislocation lines from the interface, but we shall see that other stress components are more sensitive to the heterogeneity even for model B.

The shear stress component σ_{xz} is shown in Fig. 4: in Fig. 4(h) the solution is shown for a homogeneous unbounded medium with uniform rigidity μ_1. In Figs 4(a) and (b) the complete solutions are shown for model A and B respectively. In Figs 4(c) and (d) the opposite of the Galerkin contribution ($-\sigma_{xz}^{G}$) is shown for models A and B. In Fig. 4(c) we observe an opposite behaviour with respect to the component σ_{zz}: here the stress (in absolute value) is lowered in the softer half-space 2 and enhanced in the harder half-space 1. Again, the large Galerkin contribution in model A is due to terms becoming singular when z and z_0 approach zero. Interesting differences appear also in model B, since the shear component σ_{xz}^{G} is now significant (Fig. 4d) near the interface. This may be interpreted as due to the bending of the interface, as discussed below.

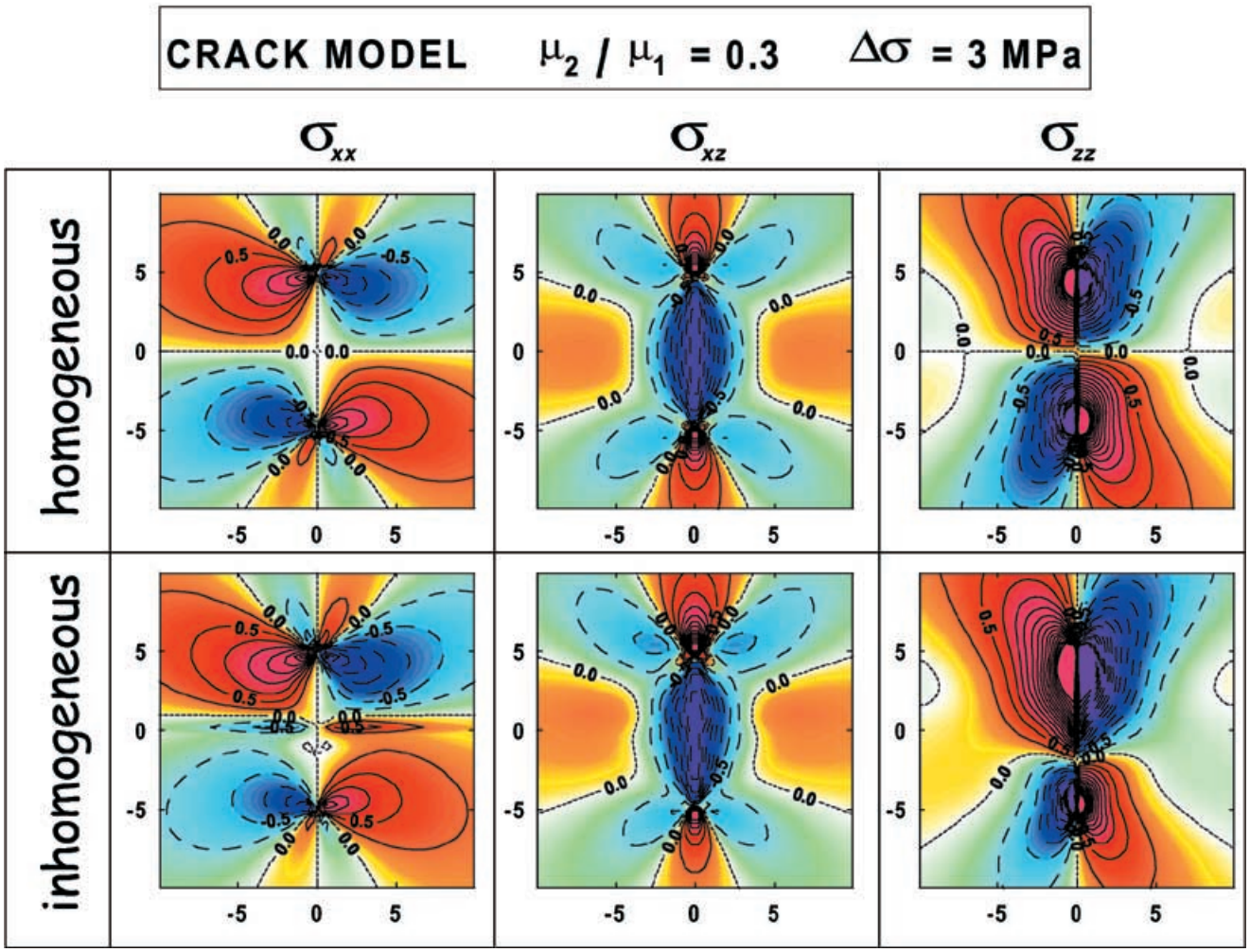

Figure 7. Map of the stress components σ_{xx}, σ_{xz} and σ_{zz} relative to the crack model C, in the homogeneous medium with $\mu_2 = \mu_1 = 30$ GPa (top panels) and in the inhomogeneous medium with $\mu_1 = 30$ GPa, $\mu_2 = 0.3\mu_1$ (bottom panels). A constant stress drop $\Delta\tau_{xz} = 3$ MPa is assigned in both cases and the solution is found in terms of a continuous distribution of edge dislocations. The crack surface is $-h/2 < z < +h/2$ with $h = 10$ km.

In Fig. 5 the discontinuous stress component σ_{xx} is shown. In Fig. 5(h) the solution is shown for a homogeneous unbounded medium with uniform rigidity μ_1. In Figs 5(a) and (b) the complete solutions are shown for model A and B respectively. In Model A we see that contour lines of σ_{xx} on the hard side of the interface are much wider than in the homogeneous medium (Fig. 5h), showing that the presence of the softer medium beyond the interface enhances this stress component significantly. In model B (Fig. 5b) this effect is even higher and two lobes containing relative maxima of $|\sigma_{xx}|$ are found on the hard side of the interface: these lobes reach horizontal distances comparable with the vertical extension of the dislocation surface. Figs 5(c) and (d) show $-\sigma_{xx}^G$ (the opposite of the Galerkin contributions) for model A and B, respectively. In model A (Fig. 5c) a complex pattern appears near the interface and near the dislocation surface, which lowers the absolute value of stress on the harder side of the interface and increases it on the softer side. However, at large distances from the dislocation surface, along the interface, non-negligible Galerkin contributions increase the absolute value of stress on both sides of the interface, giving rise to the elongated stress contours of Fig. 5(a). Galerkin contributions are very significant particularly for model B (Fig. 5d) along the interface and up to considerable distances from the dislocation surface. As a result, the complete stress component σ_{xx} reverts its sign on the harder side of the interface, its absolute value increases on the softer side and the overall stress pattern changes appreciably. These high-stress lobes can be interpreted in terms of the bending of the interface accompanying the dislocation slip, which gives rise to compression in half-space 1 on the concave side of the boundary and to extension on the convex side (see Fig. 2b). The presence of similar lobes with the same sign (but with much less amplitudes) on the softer side of the interface can be interpreted as due to the softer medium being dragged by the harder medium in the x-direction, following to the boundary conditions of displacement continuity. This qualitative interpretation is supported from the consideration that σ_{xx} depends mostly on $\frac{\partial}{\partial x}u_x$ (and on $\frac{\partial}{\partial z}u_z$, but to a lesser extent) and the former must be continuous across the interface, so that its contribution to σ_{xx} must be discontinuous but with the same sign.

Next we study the location and intensity of the two lobes of stress concentration for the σ_{xx} component in cases A and B: how do they change with the rigidity contrast $m = (\mu_1 - \mu_2)/\mu_1$ and with the position of the dislocation lines? In Fig. 6(a) model B is considered for a dislocation surface which cuts symmetrically across the interface (similar to model B of Fig. 5): the maximum amplitude of the Galerkin component over the interface $z = 0$ is shown, normalized to $\mu_1 b/h$, a representative stress drop value, where $h = 10$ km is the vertical extension of the dislocation surface $-h/2 < z < h/2$. The position of the stress extrema are steady while changing m. Employing the same parameters as in Fig. 5(b) the extrema are found in $x = \pm 2.88$ km, $z = 0^+$ km, independently of the value of m. We note that the intensity increases while decreasing the rigidity ratio and the maximum stress concentration is obtained for vanishing μ_2.

In Fig. 6(b) the maximum absolute value of the Galerkin component σ_{xx}^G is plotted as function of the extension of the dislocation surface: the lower dislocation line is fixed in $z_0 = 10$ km below the interface, in half-space 1, while the position of upper dislocation line is in $z_0 - h$ with h increasing from 1 km to 24 km. The stress singularity in $h = 10$ km is connected with the already mentioned singularities of Galerkin contributions when a dislocation line gets close to the interface. This stress maximum increases but is localized within a shrinking area while h approaches 10 km from below (model A), until the upper dislocation line enters into half-space 2 (model B) and a wide lobe of relatively high stress is attained, nearly independent of h, when the dislocation surface extends significantly into half-space 2. It may be mentioned that the stress maximum reverts its sign when the dislocation surface crosses the interface, as appears from Figs 5(c) and (d). The asymmetry of Fig. 6(b) indicates that the wide lobes of high stress appear only after the dislocation surface has crossed the interface.

In Fig. 7 the stress components are plotted for a crack model (model C) with constant stress drop $\Delta\tau_{xz} = 3$ MPa prescribed over the crack plane ($\Delta\tau$ is employed to denote the stress drop in order to avoid confusion with the stress discontinuity $\Delta\sigma$ appearing in eq. (7)). These maps are dominated by the singularities present at crack tips, but the most interesting differences with respect to the homogeneous medium are still the two stress lobes of σ_{xx} in the proximity of the interface $z = 0$, where this stress component reverts its sign with respect

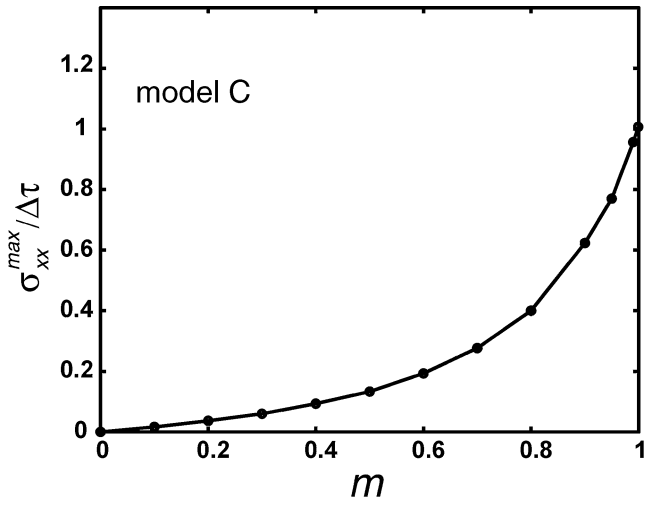

Figure 8. Maximum absolute value of the stress component σ_{xx}, computed over the interface for the crack model of Fig. 7. Stress values are normalized to the stress drop $\Delta\tau = 3$ MPa.

to the homogeneous medium. Thus, the presence of these high stress lobes in the edge dislocation problem is not model dependent, rather it is strictly related to the presence of a welded contact between two media with different elastic properties.

It is interesting to note that, in the tensile dislocation problem, much lower and narrower lobes of stress concentration in the σ_{xx} component are present in the dislocation solution with constant Burger's vector (see Fig. 5b of Bonafede & Rivalta 1999a) while larger concentrations, similar to the present ones, were present in the tensile crack model with constant overpressure (see Fig. 11b of Bonafede & Rivalta 1999b). The reason for this different behaviour can be found in the different geometry of the two problems: in the tensile problem the interface warps significantly if the fracture opens wider in the softer part of the medium, and this happens in a crack model (see Figs 8b and 9 of Bonafede & Rivalta 1999b) but not in a dislocation model with constant Burgers vector. In the dip-slip problem, on the other side, the slip on the fracture plane is normal to the interface $z = 0$, so that it warps already when the Burger's vector b is constant.

In Fig. 8 the maximum value of the Galerkin contribution for model C, computed in $z = 0^+$, is plotted versus the rigidity contrast $m = (\mu_1 - \mu_2)/\mu_1$ for the crack model C of Fig. 7. This plot shows differences with respect to model B (Fig. 6a), since the stress concentration

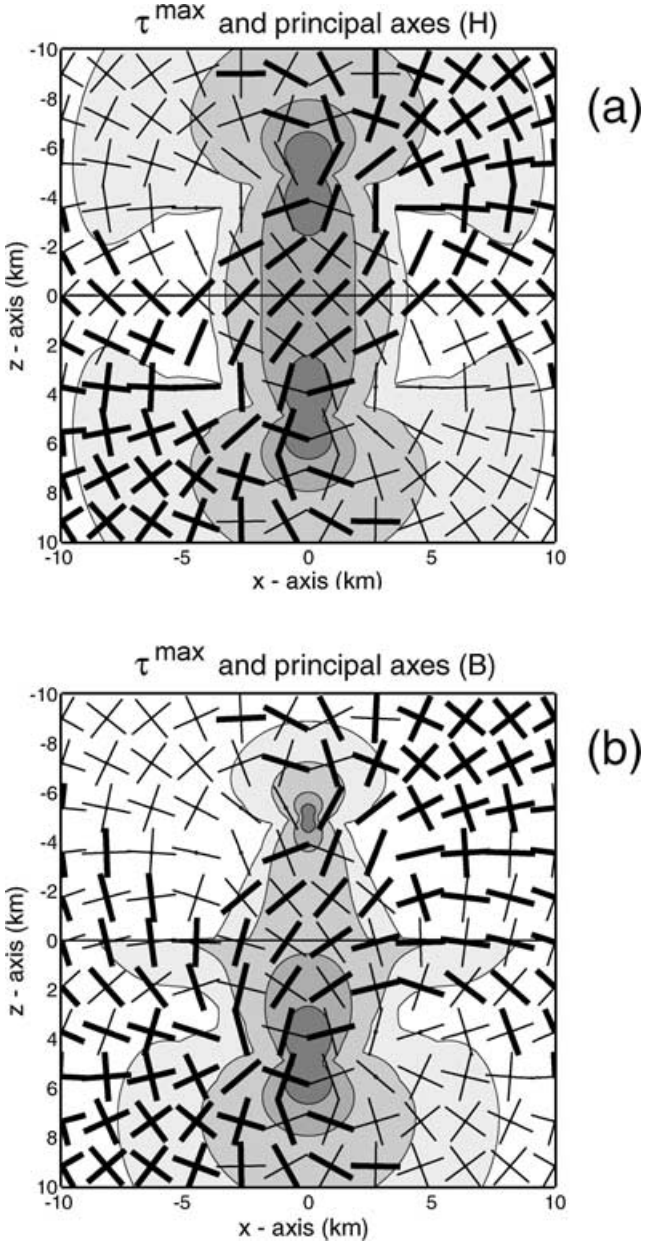

Figure 9. Map of the principal stress directions σ_1 and σ_3, relative to the dislocation model, in the homogeneous medium (h) with $\mu_2 = \mu_1 = 30$ GPa (a) and in the inhomogeneous medium (model B) with $\mu_1 = 30$ GPa, $\mu_2 = 0.3\mu_1$ (b). The value of $\tau^{\max} = \frac{\sigma_1 - \sigma_3}{2}$ is contoured in the background to show the maximum deviatoric stress (contour levels refer to 1, 2, 5, 10 bar). Thick segments indicate compression and thin segments tension. Where two segments appear, the intermediate principal stress is in the y-direction, orthogonal to the plane of the figure. Where only one segment appears, the intermediate principal stress is orthogonal to it in the plane of the figure and the other principal axis (maximum or minimum) is in the y-direction.

grows slower at first (at low m values) and then faster. It may be worthwhile mentioning that the position of the extrema is not fixed in the crack model, since it recedes from $x = 2.13$ km (for low rigidity contrast) to $x = 1.77$ km (for high rigidity contrast).

In Figs 9(a) and (b) the principal stress directions are plotted for the homogeneous case (H) and for model B. In both pictures the value of the maximum shear stress $\frac{\sigma_1 - \sigma_3}{2}$ is contoured in background. Compressive axes are indicated by thick segments and tensional axes through thin segments. The rigidity discontinuity affects in particular the proximity of the interface: both maximum shear stress and the directions of the principal axes show a different configuration in presence of a material discontinuity.

Looking at the principal axes plotted along the interface, in $z = 0^+$ (i.e. within the harder medium in panel B), we see that the maximum shear stress is typically at 45° with respect to the coordinate axes in the homogeneous medium (H). If we assume that the initial stress present before the dislocation event, was a single shear component $\tau^0_{xz} = \tau^0_{zx}$, we easily acknowledge that the induced shear stress in the homogeneous model goes mostly to release the initial stress, but this is not the case for the heterogeneous model, within the lateral lobes: the initial stress τ^0_{xz} has no shear component on its principal planes which dip at 45°. The large variation in the deviatoric stress and the directions of the principal axes thus suggest that structural discontinuities may become preferential sites of secondary rupture events.

CONCLUSIONS

In conclusion, the results of the present work show that, in presence of discontinuities of the elastic parameters, the displacement and stress fields change significantly with respect to homogeneous media: elastic discontinuities act as stress attractors, particularly for the component σ_{xx}. Stress concentrations appear both in dislocation models A and B and in the crack model C. These results differ considerably from tensile (mode I) and screw (mode III) dislocations models in layered media (Bonafede & Rivalta 1999a, 1999b; Bonafede *et al.* 2002).

The results obtained here and in the previous papers give a preliminary insight into the question of how inhomogeneities can affect the stress field generated by faulting or by dyke injection: the answer is that inhomogeneities are responsible for significant changes with respect to homogeneous models, providing stress concentrations which amount to significant fractions of the stress drop and extend along the elastic discontinuities up to distances comparable to the vertical extension of the dislocation surface, particularly when faults cut across the discontinuities. Stress components which do not need be continuous across the interface are typically most affected by the presence of elastic inhomogeneities.

Stress concentration along interfaces is particularly high when the rigidity contrast is high. Very high rigidity contrasts are seldom found in the crust as far as the elastic behaviour is considered, but higher contrasts of effective rigidities can be obtained if a viscoelastic rheology is considered: for instance, the SLS rheology often employed to account for seismic wave attenuation, accounts for long term rigidity which may be significantly lower than the short term rigidity.

As a result, the interpretation of triggered seismicity in terms of stress induced by slip on nearby faults or by dyke injection in volcanic regions should take the elastic (and rheological) structure of the medium into account.

However, proceeding analytically beyond the simple models described in this paper becomes soon awkward: the simple addition of a free surface boundary conditions to the present model would make the analytic inversion of Galerkin components extremely cumbersome and it seems advisable to resort to numerical methods. The present solutions are in any case useful in testing numerical models, (e.g. to deploy suitable meshes in finite element models) which may provide the displacement and stress fields generated by a dip-slip fault embedded in a more complex heterogeneous medium. Exact analytical solutions are also important because they yield the singular part of the integral kernels appearing in crack problems, and we have seen that singularities are present at crack tips and at the intersection of the crack surface with the welded interface.

ACKNOWLEDGMENTS

Useful suggestions by anonymous referees contributed to improve the paper and are gratefully acknowledged. Research funded by the Italian Ministry of the University and Scientific and technological research (MURST).

REFERENCES

Bonafede, M. & Danesi, S., 1997. Near-field modifications of stress induced by dyke injection at shallow depth, *Geophys. J. Int.,* **130,** 433–448.

Bonafede, M. & Rivalta, E., 1999a. The tensile dislocation problem in a layered elastic medium, *Geophys. J. Int.,* **136,** 341–356.

Bonafede, M. & Rivalta, E., 1999b. On tensile cracks close to and across the interface between two welded elastic half spaces, *Geophys. J. Int.,* **138,** 410–434.

Bonafede, M., Parenti, B. & Rivalta, E., 2002. On strike slip faulting in layered media, *Geophys. J. Int.,* in press.

Crouch, S.L. & Starfield, A.M., 1990. *Boundary Element Methods in Solid Mechanics,* Unwin Hyman Inc., London.

Dahm, T., 1996. Elastostatic simulation of dislocation sources in heterogeneous stress fields and multilayered media having irregular interfaces, *Phys. Chem. Earth,* **21,** 241–245.

Erdogan, F., Gupta, G.D. & Cook, T.S., 1973. Numerical solution of singular integral equations, in *Mechanics of Fracture, Vol. I,* pp. 368–425, ed. Sih G.C., Noordhoff, Leyden.

Fung, Y.C., 1965. *Foundations of Solid Mechanics,* Prentice Hall, Englewood Cliffs, New Jersey.

Harris, R.A., 1998. Introduction to special section: stress triggers, stress shadows and implications for seismic hazard, *J. geophys. Res.,* **103,** 24 347–24 358.

King, G.C.P., Stein, R.S. & Lin, J., 1994. Static stress change and the triggering of earthquakes, *Bull. seism. Soc. Am.,* **84,** 935–953.

Landau, L.D. & Lifschitz, E., 1967. *Théorie de l'élasticité,* Éditions Mir, Moscou.

Maruyama, T., 1964. Statical elastic dislocations in an infinite and semi-infinite medium, *Bull. Earthq. Res. Inst. Tokyo Univ.,* **42,** 289–368.

McTigue, D.F. & Segall, P., 1988. Displacements and tilts from dip-slip faults and magma chambers beneath irregular surface topography, *Geophys. Res. Lett.,* **15,** 601–604.

Okada, Y., 1992. Internal deformation due to shear and tensile faults in a half-space, *Bull. seism. Soc. Am.,* **82,** 1018–1040.

Roth, F., 1990. Subsurface deformations in a layered half-space, *Geophys. J. Int.,* **103,** 147–155.

Rundle, J.B., 1980. Static elastic-gravitational deformation of a layered half-space by point couple sources, *J. geophys. Res.,* **85,** 5355–5363.

Rybicki, K.R., 1971. The elastic residual field of a very long strike-slip fault in the presence of a discontinuity, *Bull. seism. Soc. Am.,* **61,** 79–92.

Rybicki, K.R., 1973. Analysis of aftershocks on the basis of dislocation theory, *Phys. Earth planet. Inter.,* **7,** 409–422.

Savage, W.Z. & Swalfs, H.S., 1986. Tectonic and gravitational stress in long symmetric ridges and valleys, *J. geophys. Res.,* **91,** 3677–3685.

Singh, S.J., 1970. Static deformation of a multilayered half-space by internal sources, *J. geophys. Res.,* **75,** 3257–3263.

Stein, R.S., King, G.C.P. & Lin, J., 1992. Change in failure stress on the southern San Andreas fault system caused by the 1992 magnitude = 7.4 Landers earthquake, *Science,* **258,** 1328–1332.

APPENDIX A: THE FUNCTIONS I_{ij} AND Y_{ij}

The integrals $I_{ij}(x, z; z_0)$ appearing in (27–28) and (31–33) are defined in Bonafede & Rivalta (1999a) and are reproduced below for ease of reference:

$$
\begin{aligned}
I_{11} &= \frac{z_0+z}{\left[x^2+(z+z_0)^2\right]}, & I_{12} &= \frac{z\left[(z+z_0)^2-x^2\right]}{\left[x^2+(z+z_0)^2\right]^2}, & I_{13} &= \frac{z_0\left[(z+z_0)^2-x^2\right]}{\left[x^2+(z+z_0)^2\right]^2}, & I_{14} &= \frac{2zz_0(z_0+z)\left[(z+z_0)^2-3x^2\right]}{\left[x^2+(z+z_0)^2\right]^3},\\
I_{21} &= \frac{z_0-z}{\left[x^2+(z-z_0)^2\right]}, & I_{22} &= \frac{z\left[(z-z_0)^2-x^2\right]}{\left[x^2+(z-z_0)^2\right]^2}, & I_{23} &= \frac{z_0\left[(z-z_0)^2-x^2\right]}{\left[x^2+(z-z_0)^2\right]^2}, & I_{24} &= \frac{2zz_0(z_0-z)\left[(z-z_0)^2-3x^2\right]}{\left[x^2+(z-z_0)^2\right]^3},\\
I_{31} &= \frac{x}{\left[x^2+(z+z_0)^2\right]}, & I_{32} &= \frac{2xz(z_0+z)}{\left[x^2+(z+z_0)^2\right]^2}, & I_{33} &= \frac{2xz_0(z_0+z)}{\left[x^2+(z+z_0)^2\right]^2}, & I_{34} &= \frac{2zz_0x\left[3(z_0+z)^2-x^2\right]}{\left[x^2+(z+z_0)^2\right]^3},\\
I_{41} &= \frac{x}{\left[x^2+(z-z_0)^2\right]}, & I_{42} &= \frac{2xz(z_0-z)}{\left[x^2+(z-z_0)^2\right]^2}, & I_{43} &= \frac{2xz_0(z_0-z)}{\left[x^2+(z-z_0)^2\right]^2}, & I_{44} &= \frac{2zz_0x\left[3(z_0-z)^2-x^2\right]}{\left[x^2+(z-z_0)^2\right]^3},
\end{aligned}
\tag{A1}
$$

The functions $Y_{ij}(x, z; z_0) = \int I_{ij}\, dx + c$ appearing in (26) and (29) are given below (c is a constant chosen as to yield continuity of the displacement field over the plane $z = 0$):

$$
\begin{aligned}
Y_{11} &= \arctan\frac{z_0+z}{x} - \frac{\pi}{2}\,\mathrm{sgn}(xz_0), & Y_{12} &= \frac{zx}{x^2+(z+z_0)^2}, & Y_{13} &= \frac{z_0x}{x^2+(z+z_0)^2}, & Y_{14} &= \frac{2zz_0x(z_0+z)}{\left[x^2+(z+z_0)^2\right]^2},\\
Y_{21} &= \arctan\frac{z_0-z}{x} - \frac{\pi}{2}\,\mathrm{sgn}(xz_0), & Y_{22} &= \frac{zx}{x^2+(z-z_0)^2}, & Y_{23} &= \frac{z_0x}{x^2+(z-z_0)^2}, & Y_{24} &= \frac{2zz_0x(z_0-z)}{\left[x^2+(z-z_0)^2\right]^2},\\
Y_{31} &= \ln\sqrt{\frac{x^2+(z+z_0)^2}{z_0^2}}, & Y_{32} &= -\frac{z(z_0+z)}{x^2+(z+z_0)^2}, & Y_{33} &= -\frac{z_0(z_0+z)}{x^2+(z+z_0)^2}, & Y_{34} &= \frac{zz_0\left[x^2-(z_0+z)^2\right]}{\left[x^2+(z+z_0)^2\right]^2},\\
Y_{41} &= \ln\sqrt{\frac{x^2+(z-z_0)^2}{z_0^2}}, & Y_{42} &= -\frac{z(z_0-z)}{x^2+(z-z_0)^2}, & Y_{43} &= -\frac{z_0(z_0-z)}{x^2+(z-z_0)^2}, & Y_{44} &= \frac{zz_0\left[x^2-(z_0-z)^2\right]}{\left[x^2+(z-z_0)^2\right]^2}.
\end{aligned}
\tag{A2}
$$

In Y_{11} and Y_{21} the function $\mathrm{sgn}(xz_0) = \pm 1$ according to whether the argument xz_0 is positive or negative.